

Challenging Adiabatic Time-dependent Density Functional Theory with a Hubbard Dimer: The Case of Time-Resolved Long-Range Charge Transfer

Johanna I. Fuks¹ and Neepa T. Maitra¹

¹*Department of Physics and Astronomy, Hunter College and the City University of New York, 695 Park Avenue, New York, New York 10065, USA*

(Dated: May 7, 2021)

We explore an asymmetric two-fermion Hubbard dimer to test the accuracy of the adiabatic approximation of time-dependent density functional theory in modelling time-resolved charge transfer. We show that the model shares essential features of a ground state long-range molecule in real-space, and by applying a resonant field we show that the model also reproduces essential traits of the CT dynamics. The simplicity of the model allows us to propagate with an “adiabatically-exact” approximation, i.e. one that uses the exact ground-state exchange-correlation functional, and compare with the exact propagation. This allows us to study the impact of the time-dependent charge-transfer step feature in the exact correlation potential of real molecules on the resulting dynamics. Tuning the parameters of the dimer allows a study both of charge-transfer between open-shell fragments and between closed-shell fragments. We find that the adiabatically-exact functional is unable to properly transfer charge, even in situations where the adiabatically-exact resonance frequency is remarkably close to the exact resonance, and we analyze why.

I. INTRODUCTION

The transfer of an electron across a molecule is an essential process in biology, chemistry, and physics, that needs to be accurately described in order to computationally model phenomena in many topical applications, e.g. photovoltaics, vision, photosynthesis, molecular electronics, and the control of coupled electron-ion dynamics by strong lasers (e.g. Refs [1–7]). For most of these applications, a time-resolved picture of the charge transfer (CT) is extremely useful, and often necessary, as has been stressed in recent work, and the correlation between electrons as well as between electrons and ions play a crucial role [8]. The systems are large enough that time-dependent density functional theory (TDDFT) is the only computationally feasible approach [9–11]. It is well-known that the standard functional approximations considerably underestimate CT excitations, and there has been intense development of improved functionals for this; in particular the optimally tuned hybrids present a useful non-empirical approach [12]. However the transfer of one electron from one region of space to another is clearly a non-perturbative process and calls for calculations that go beyond linear response and excitations. The success of TDDFT to date rests on its performance in the linear regime, however the theory applies also to dynamics far from equilibrium. The performance of functionals for CT in this regime paints a more hazy picture: there have been calculations in good agreement with experiment (e.g. Ref. [6]) but failures have been reported too [13]. It would be fair to say that it is not always clear to what accuracy the TDDFT results can be trusted. Part of the problem is that there are very few alternate practical computational methods for correlated electronic dynamics to test against. Calculations on simplified model systems that can be solved exactly, e.g. two-electron systems in one-dimension, have high-

lighted prominent features that the approximate functionals lack, not just for CT dynamics [14], but also more generally in the non-linear regime [15–18]. The errors that result from the lack of these features appear to be sometimes very significant, and other times less so.

TDDFT in practise is almost always synonymous with adiabatic TDDFT, certainly in the non-linear regime. That is, the Kohn-Sham (KS) system is propagated using an adiabatic exchange-correlation potential, where the evolving density at time t is input into a ground-state (gs) functional: $v_{xc}^A[n; \Psi_0, \Phi_0](\mathbf{r}, t) = v_{xc}^{gs}[n(t)](\mathbf{r})$. There are two distinct sources of error in such an approximation: one is from the choice of the gs functional approximation, while the other is the adiabatic approximation itself. To separate these the *adiabatically-exact* (AE) approximation [18] is defined: the instantaneous density is input into the exact gs functional, $v_{xc}^{AE}[n; \Psi_0, \Phi_0](\mathbf{r}, t) = v_{xc}^{AE}[n](\mathbf{r}, t) = v_{xc}^{exact\ gs}[n(t)](\mathbf{r})$. This approximation neglects memory-dependence that the exact functional is known to possess (dependence on the density’s history and true and KS initial states Ψ_0 and Φ_0) but is fully non-local in space, and, if the true and KS states at time t were actually gs’s of some potential, it would be exact at time t .

Since the exact gs exchange-correlation functional is not known, even for one-dimensional two electron systems, $v_{xc}^{AE}[n](\mathbf{r}, t)$ must be found via a numerical scheme, of an inverse problem type. A handful of papers [14, 17, 18] have found $v_{xc}^{AE}[n](\mathbf{r}, t)$ using an iterative scheme for some model systems: The exact density $n(t)$, found by solving the interacting Schrödinger equation, provides the input to an iterative procedure that finds at each t of interest the interacting and non-interacting gs’s of density $n(t)$, along with the potential in which they are the gs. Then, $v_{xc}^{AE}[n(t)](\mathbf{r}) = v_{ext}^{exact\ gs}[n(t)](\mathbf{r}) - v_s^{exact\ gs}[n(t)](\mathbf{r}) - v_H[n(t)](\mathbf{r})$ where $v_H[n](\mathbf{r})$ is the electrostatic Hartree potential. In most

cases studied so far the AE potential $v_{xc}^{AE}[n](\mathbf{r}, t)$ has been evaluated on the exact density $n(t)$, and compared with the exact (memory-dependent) exchange-correlation potential $v_{xc}[n, \Psi_0, \Phi_0](\mathbf{r}, t)$ at that time, to analyze how good the AE approximation is, what features of the exact potential are missing, etc. In one case, the AE potential was used to self-consistently propagate the KS orbitals, using at each time-step, the AE potential evaluated on the self-consistent instantaneous density. Such a propagation provides a more useful assessment of the accuracy of the AE, as it measures directly the impact of the AE on the resulting dynamics. For example, it is possible that some features that might make the AE potential look significantly different than the exact, may in fact have a limited effect on the propagation. However, self-consistent AE propagation clearly requires much more numerical effort, as many iterations need to be performed at every time-step to find the potential to propagate in, and it has only been done in a few examples [18–20] in one-dimensional model systems. In regions where the density becomes too small, the inversion becomes unstable and noisy.

In particular, for CT dynamics it is particularly challenging to converge the iterative density-inversion scheme due to the very low density region between the atoms. Yet, such a calculation is of great interest for CT dynamics: not only because of its significance in the phenomena mentioned earlier, but also because it is known the exact functional develops features that the usual approximations lack. Ref. [14] showed that for a two-electron model molecule composed of closed-shell atoms and driven at the CT resonance, a step associated with the CT process gradually builds up over time in the exact correlation potential. A dynamical oscillatory step is superimposed on this (see Refs. [17, 21]), and is a generic feature of non-linear dynamics, not only in CT dynamics, that has a non-adiabatic density-dependence. The AE approximation fails to capture the dynamical step but, when evaluated on the *exact* density, does yield a CT step although of a smaller size than the exact. Such steps require functionals with a spatially non-local dependence on the density. The available approximations do not yield any step structure whatsoever: the dismal failure of ALDA, ASIC-LDA, and AEXX, none of which contain any step in the correlation potential, to transfer any charge was shown (Fig 3 of Ref. [14]) and attributed to this lack of step structure. We expect some blame must go to the adiabatic approximation itself, but a question arises: is the partial step of the AE approximation enough to give a reasonable description of the CT dynamics? If yes, this would greatly simplify the on-going search for accurate functionals for non-perturbative CT: it would mean that one does need to build in spatial non-local density-dependence into the correlation functional approximation, but that one could get away with a time-local, i.e. adiabatic approximation. To answer the question, we would need to propagate with the AE self-consistently, but as discussed above,

this procedure is numerically very challenging for CT dynamics. In a recent short paper [22], we have shown that the answer is no, by studying CT dynamics in a two-fermion asymmetric Hubbard dimer, which shares the essential features of CT dynamics with real-space molecules. Due to the small Hilbert space of the dimer the exact gs functional can be found via a constrained search, and then used in $v_{xc}^{AE}(t)$ to self-consistently propagate the system. No iterative scheme is needed because the exact functional form of the gs Hartree-exchange-correlation (HXC) potential is known. This enabled us to assess errors in the adiabatic approximation for CT dynamics independently of those resulting from errors in the gs approximation used. In this paper we give more details on the dimer model, and the procedure followed. Like in Ref. [22], we study both the cases of resonant CT between closed-shells and between open-shells, by tuning the potential-difference between the two sites. However, unlike Ref [22], we choose this asymmetry such that the CT state of the first case has a very similar density as the gs of the second, and vice-versa. Although this choice leads to the exact density-dynamics in one case being a time-reversed version of the dynamics in the other case, we find the AE dynamics does not have this property. The AE approximation in the closed-shell case is better for longer than for the open-shell case, where it fails almost immediately; yet in either case, it fails to properly transfer the charge. The hope that the step seen in the AE approximation evaluated on the exact density, albeit smaller than the exact, is enough to do a reasonable job for CT processes is dashed. A further result is an expression for the interacting frequencies of the system in terms of the KS ones and the HXC kernel. Using this, we compare the exact resonant frequency of the interacting system with that predicted by the AE approximation.

In Section II we introduce the model, its ground-state energies and potentials, and the exact time-dependent KS potential. In Section III, we present the parameters used to study CT between closed-shells, give details of the eigenstates of the interacting and KS systems, and propagate the system with a resonant field to induce Rabi oscillations between the ground and CT excited state. We compare the exact propagation with that resulting from the AE propagation and discuss features of the potentials. Section IV contains the analogous analysis for the case of CT between open-shells. In Section V we derive a formula for the interacting frequencies of the system in terms of the KS ones and the HXC kernel. This is used to find the AE resonant frequency, and compare with the exact in each case.

II. THE MODEL

The Hamiltonian of the two-site interacting Hubbard model with on-site repulsion U and hopping parameter







site L	site R	
		$\frac{1}{\sqrt{2}} [\uparrow, \downarrow \rangle - \downarrow, \uparrow \rangle]$
		$ \uparrow \downarrow, 0 \rangle$
		$ 0, \uparrow \downarrow \rangle$

FIG. 1. The three states pictured form a complete basis of the singlet sector of the Hubbard dimer.

T [22–30] reads:

$$\hat{H} = -T \sum_{\sigma} \left(\hat{c}_{L\sigma}^{\dagger} \hat{c}_{R\sigma} + \hat{c}_{R\sigma}^{\dagger} \hat{c}_{L\sigma} \right) + U (\hat{n}_{L\uparrow} \hat{n}_{L\downarrow} + \hat{n}_{R\uparrow} \hat{n}_{R\downarrow}) + \frac{\Delta v(t)}{2} (\hat{n}_L - \hat{n}_R), \quad (1)$$

where $\hat{c}_{L(R)\sigma}^{\dagger}$ and $\hat{c}_{L(R)\sigma}$ are creation and annihilation operators for a spin- σ electron on the left(right) site $L(R)$, respectively, and $\hat{n}_{L(R)} = \sum_{\sigma=\uparrow,\downarrow} \hat{c}_{L(R)\sigma}^{\dagger} \hat{c}_{L(R)\sigma}$ are the site-occupancy operators.

The occupation difference $\langle \hat{n}_L - \hat{n}_R \rangle = \Delta n$ represents the dipole in this model, $d = \Delta n$, and is the main variable [28]; the total number of fermions is fixed at $N = 2$. A static potential difference, $\Delta v^0 = \sum_{\sigma} (v_{L\sigma}^0 - v_{R\sigma}^0)$, renders the Hubbard dimer asymmetric. The total external potential $\Delta v(t)$ is given by $\Delta v(t) = \Delta v^0 + 2\mathcal{E}(t)$, where the last term represents an electric field that we will tune to induce CT between the sites. An infinitely long-range molecule is modelled by $T/U \rightarrow 0$: in our calculations, we fix the interaction strength to be unity, $U = 1$ and make the hopping parameter T small, corresponding to a large separation between the sites (equivalent to the strongly correlated limit $U/T \rightarrow \infty$). We use $\hbar = e = 1$ throughout, and all energies are given in units of U .

The singlet sector of the two-electron vector space is three-dimensional (depicted in Fig. 1),

$$|\Psi_1\rangle = \frac{1}{\sqrt{2}} \left(\hat{c}_{1\uparrow}^{\dagger} \hat{c}_{2\downarrow}^{\dagger} - \hat{c}_{1\downarrow}^{\dagger} \hat{c}_{2\uparrow}^{\dagger} \right) |0\rangle = \frac{1}{\sqrt{2}} [| \uparrow, \downarrow \rangle - | \downarrow, \uparrow \rangle] \quad (2)$$

$$|\Psi_2\rangle = \hat{c}_{1\uparrow}^{\dagger} \hat{c}_{1\downarrow}^{\dagger} |0\rangle = | \uparrow \downarrow, 0 \rangle \quad (3)$$

$$|\Psi_3\rangle = \hat{c}_{2\uparrow}^{\dagger} \hat{c}_{2\downarrow}^{\dagger} |0\rangle = | 0, \uparrow \downarrow \rangle \quad (4)$$

For fixed T/U a constrained search over all gs wavefunctions $|\Psi\rangle = a_1|\Psi_1\rangle + a_2|\Psi_2\rangle + a_3|\Psi_3\rangle$ that yield a given Δn [32, 33] can be straightforwardly performed

due to the small size of the Hilbert space. This results in the Hohenberg-Kohn (HK) energy functional [31–33]:

$$F_{HK}[\Delta n] = \min_{\Psi \rightarrow \Delta n} \langle \Psi_{\Delta n} | \hat{T} + \hat{U} | \Psi_{\Delta n} \rangle = E_{\text{HXC}}[\Delta n] + T_s[\Delta n], \quad (5)$$

where \hat{T} and \hat{U} are the first two terms in Eq. (1), $T_s[\Delta n] = \min_{\Phi \rightarrow \Delta n} \langle \Phi_{\Delta n} | \hat{T} | \Phi_{\Delta n} \rangle$ is the non interacting kinetic energy, and Φ denotes a single Slater determinant. $E_{\text{HXC}}[\Delta n]$ is the HXC energy functional, which must in practise be approximated for real systems, but here for the Hubbard model we can compute it explicitly exactly numerically. The HK functional $F_{HK}[\Delta n]$ completely determines the gs energy E_{gs} ,

$$E_{\text{gs}} = \min_{\Delta n} \left(F_{\text{HK}}[\Delta n] + \frac{\Delta v^0}{2} \Delta n \right). \quad (6)$$

The gs occupation difference Δn_{gs} of all possible asymmetric (and symmetric) Hubbard dimers is determined by $\frac{\partial F_{\text{HK}}}{\partial \Delta n} \big|_{\Delta n_{\text{gs}}} = -\frac{\Delta v^0}{2}$.

The minimization Eq. (5) was carried out in Mathematica; the resulting discrete function $F_{\text{HK}}^j(\Delta n_j)$ was fitted and derived using splines to obtain the exact gs HXC potential $\Delta v_{\text{HXC}}^{\text{gs}}[\Delta n] = 2 \frac{\partial (F_{\text{HK}}[\Delta n] - T_s[\Delta n])}{\partial \Delta n}$ (see Fig. 2). (The factor 2 in the right hand side of Eq. (7) results from expressing the energy functional in terms of the variable $\Delta n = n_L - n_R$, namely $\Delta v_{\text{C}}^{\text{gs}}[\Delta n] = v_{\text{C}}^L[\Delta n] - v_{\text{C}}^R[\Delta n] = \frac{dE_{\text{C}}[\Delta n]}{d(\Delta n)} \frac{d\Delta n}{dn_L} - \frac{dE_{\text{C}}[\Delta n]}{d(\Delta n)} \frac{d\Delta n}{dn_R}$.)

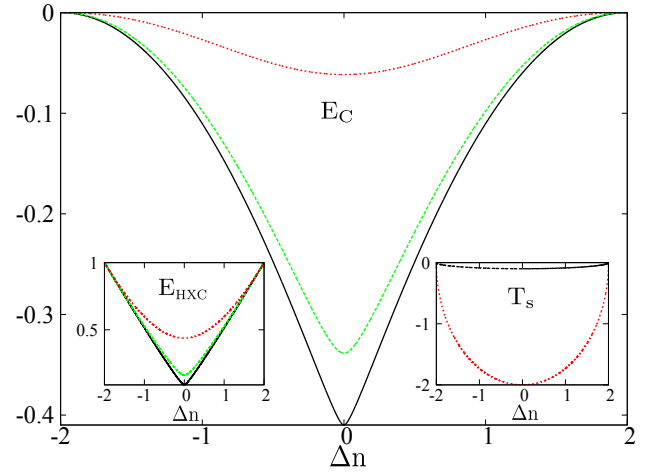


FIG. 2. Correlation energy functional $E_{\text{C}}[\Delta n]$ for $T = 1$ (red dotted) $T = 0.1$ (green dashed) and $T = 0.05$ (black solid). Insets: $E_{\text{HXC}}[\Delta n]$ (left) and non-interacting kinetic energy functional $T_s[\Delta n]$ for the same parameters. Energies are in units of U .

In Fig. 2 the different components of the energy as functions of the occupation difference Δn for different T and fixed Hubbard strength $U = 1$ are plotted. Note that the Hartree-exchange (HX) part of the energy functional is independent of T , $E_{\text{HX}}[\Delta n] = (N^2 + \Delta n^2)U/8$

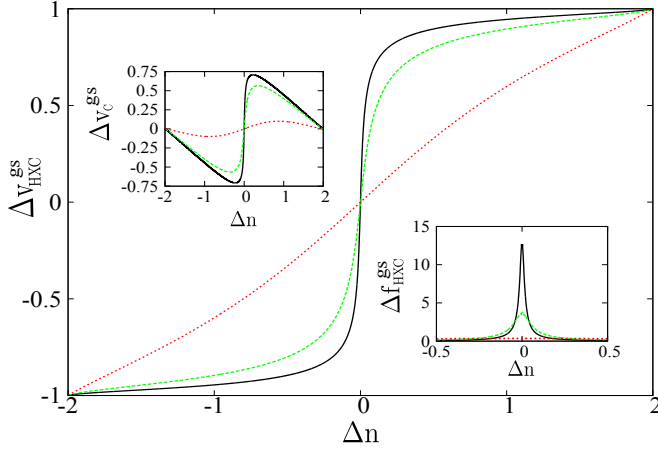


FIG. 3. Ground-state HXC potential functional $\Delta v_{\text{HXC}}^{\text{gs}}[\Delta n]$ for $T = 1$ (red dotted) $T = 0.1$ (green dashed) and $T = 0.05$ (black solid). Left inset: Ground-state correlation potential functional $\Delta v_{\text{C}}^{\text{gs}}[\Delta n]$. Right inset: $\Delta f_{\text{HXC}}^{\text{gs}}[\Delta n] = \frac{d^2 E_{\text{HXC}}[\Delta n]}{d(\Delta n)^2}$.

(with N being the number of particles) [27]. In the limit where the two electrons are sitting on the same site the HXC energy is entirely due to HX and equal to the on-site repulsion U , $E_{\text{HXC}}[\Delta n = \pm 2] = E_{\text{HX}} = U$ (see left inset in Fig. 2). The hopping parameter T plays a role as soon as the electronic density delocalizes. As shown in right inset of Fig. 2 the non-interacting kinetic energy $T_{\text{s}}[\Delta n]$ depends strongly on T .

For small occupation differences $\Delta n \rightarrow 0$ (one electron on each site), in the infinite separation limit $T/U \rightarrow 0$, the correlation energy $E_{\text{C}}[\Delta n]$ develops a discontinuity in its derivative (see Fig. 2). This discontinuity manifests in a step-like function in the correlation potential difference $\Delta v_{\text{C}}^{\text{gs}}[\Delta n] = 2 \frac{\partial \Delta E_{\text{C}}}{\partial \Delta n}$ (see left inset Fig. 3). This feature is related to the derivative discontinuity of the isolated 1-electron site for the following reason. The variable Δn plays the role of the density-variable, as well as directly giving the particle number on each site, $n_{\text{L,R}} = 1 \pm \Delta n/2$. So, in the isolated-site limit $T/U \rightarrow 0$, a variation δn near $\Delta n = 0$ can be thought of as adding(subtracting) a fraction of charge δn to the one-fermion site on the left(right):

$$2 \frac{dE_{\text{C}}[\Delta n]}{d(\Delta n)} \Big|_{\Delta n=0^+} - 2 \frac{dE_{\text{C}}[\Delta n]}{d(\Delta n)} \Big|_{\Delta n=0^-} = \Delta v_{\text{C}}^{\text{gs}}[\Delta n = 0^+] - \Delta v_{\text{C}}^{\text{gs}}[\Delta n = 0^-] \equiv 2\Delta_{\text{C}}^{\text{1-site}}(N=1) \quad (7)$$

The difference in the correlation potential as one crosses $\Delta n = 0$, therefore coincides with the derivative discontinuity at $N = 1$ of one site; the value of $\Delta_{\text{C}}^{\text{1-site}}(N=1) = U$. The discontinuity only shows up in the infinite separation limit; if instead the two sites lie closer to each other they can not be considered as two separated one-electron systems and thus moving a fraction of electron back or forth represents a smooth change in the energy.

In section III we will study CT dynamics between two closed-shell fragments (cs-cs) by applying a relatively

large static potential difference such that $\Delta n_{\text{gs}} \approx 2$. One electron will be transferred to the other site by turning on a field resonant with the CT excitation frequency. Looking at Figs. 2-3 this corresponds to scanning the densities starting at the outer right region and finishing at the central region once the CT state (consisting of two now open-shell sites) is reached. The AE propagation is performed using the exact gs HXC potential $\Delta v_{\text{HXC}}^{\text{gs}}[\Delta n]$ shown in Fig. 3, i.e. assuming that at every time t the density $\Delta n(t)$ is the gs density of some potential Δv . In section IV we study instead CT between two open-shell fragments (os-os), starting with a gs consisting of two open-shell sites each with approximately one electron ($\Delta n_{\text{gs}} \approx 0$) that evolves to a CT state with $\Delta n \approx 2$; thus scanning the densities in a “time-reversed” way compared to Sec. III, moving from the central region in Figs. 2-3 to the outer region. We have chosen the Δv^0 's such that the CT density of the cs-cs system is close to the gs density of the os-os system, $\Delta n_{\text{CT}}^{\text{cs-cs}} \approx \Delta n_{\text{gs}}^{\text{os-os}}$ and vice-versa, $\Delta n_{\text{CT}}^{\text{os-os}} \approx \Delta n_{\text{gs}}^{\text{cs-cs}}$.

A. Time-dependent Kohn-Sham potential

The KS Hamiltonian has the form of Eq. (1) but with $U = 0$ and $\Delta v(t)$ replaced by the KS potential difference,

$$\Delta v_{\text{s}}[\Delta n, \Phi(t_0)](t) = v_{\text{HXC}}[\Delta n, \Psi(t_0), \Phi(t_0)](t) + \Delta v(t), \quad (8)$$

defined such that the interacting $\Delta n(t)$ is reproduced. The exact time-dependent KS potential can be found by inversion of the time-dependent KS equations [10] assuming a doubly-occupied singlet state. This yields [29]

$$\Delta v_{\text{s}}[\Delta n, \Phi(t=0)] = - \left(\frac{\ddot{\Delta n} + (2T)^2 \Delta n}{\sqrt{(2T)^2 (4 - (\Delta n)^2) - (\dot{\Delta n})^2}} \right) \quad (9)$$

when the KS initial state is the KS gs. $\Delta n(t)$ is time-dependent non-interacting V -representable as long as the denominator in Eq. (9) does not vanish,

$$|\dot{\Delta n}| < 2T\sqrt{4 - (\Delta n)^2}. \quad (10)$$

Condition (10) fixes an upper bound to the absolute value of the link-current $|\Delta n|$, which can be identified with the sum of currents flowing along links attached to the site. On a lattice the maximum link-current depends on T (see [29] and refs. therein).

III. CLOSED-SHELL TO CLOSED-SHELL CT

To model CT between two closed-shell fragments we choose the static external potential difference in the Hubbard dimer to be $\Delta v^0 = -1.5 U$, which results in a gs with almost two fermions sitting on the left site $\Delta n_{\text{gs}} = 1.9620$ (see top left of Fig. 4). The vector space

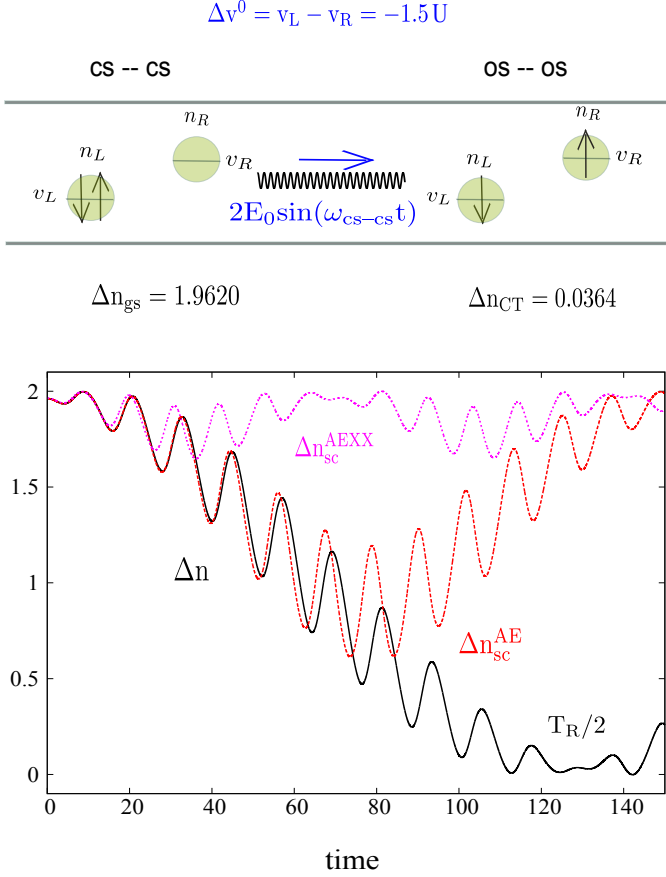


FIG. 4. Model of CT between two closed-shell fragments at large separation: a large static potential difference $\Delta v^0 = -1.5 U$ is chosen such that in the gs almost two electrons are sitting on the left site ($\Delta n_g \approx 2$) and $T/U = 0.05$. In the bottom panel the results of the propagation are shown: exact dipole $\Delta n(t)$ (black solid), self-consistent AE dipole $\Delta n_{sc}^{AE}(t)$ (red dashed) and self-consistent adiabatic EXX dipole $\Delta n_{sc}^{AEXX}(t)$ (pink dotted). Time is given in units of $1/U$, CT state is reached at $T_R/2 \approx 128/U$.

is built from the three singlet states introduced in Fig. 1 and Eqs. 4, and we shall now describe the eigenstates in detail. The interacting states in this basis were found by first computing the matrix elements of the static Hamiltonian Eq. 1 ($\mathcal{E}(t) = 0$) in basis Eqs. 4 and then diagonalizing the matrix. The calculation was performed in a self-developed code written in the second quantization formalism. The interacting gs is predominantly $|\Psi_2\rangle$:

$$|\Psi_{gs}^{cs-cs}\rangle = -0.13781 \frac{1}{\sqrt{2}} [|\uparrow, \downarrow\rangle - |\downarrow, \uparrow\rangle] + 0.99045 |\uparrow\downarrow, 0\rangle + 0.00323 |0, \uparrow\downarrow\rangle, \quad (11)$$

while the first excited state is mainly $|\Psi_1\rangle$, i.e. is a CT excitation with about one electron on each site,

$$|\Psi_{e1}^{cs-cs}\rangle = 0.990054 \frac{1}{\sqrt{2}} [|\uparrow, \downarrow\rangle - |\downarrow, \uparrow\rangle] - 0.13785 |\uparrow\downarrow, 0\rangle + 0.02809 |0, \uparrow\downarrow\rangle. \quad (12)$$

There is a second CT excited state Ψ_{e2}^{cs-cs} , dominated by $|\Psi_3\rangle$,

$$|\Psi_{e2}^{cs-cs}\rangle = -0.02827 \frac{1}{\sqrt{2}} [|\uparrow, \downarrow\rangle - |\downarrow, \uparrow\rangle] + 0.000666 |\uparrow\downarrow, 0\rangle + 0.9996 |0, \uparrow\downarrow\rangle. \quad (13)$$

The KS states Φ are obtained from diagonalization of the exact gs KS Hamiltonian, which corresponds to taking $U \rightarrow 0$ and $\Delta v = \Delta v^0 + \Delta v_{\text{HXC}}[\Delta n]$ in Eq. 1, with $\Delta v_{\text{HXC}}[\Delta n] = 2 \frac{\partial E_{\text{HXC}}[\Delta n]}{\partial \Delta n}$ and $E_{\text{HXC}}[\Delta n]$ found by constrained search as discussed in section II. The non-interacting two-electron KS gs is also predominantly $|\Psi_2\rangle$:

$$|\Phi_{gs}^{cs-cs}\rangle = 0.137236 \frac{1}{\sqrt{2}} [|\uparrow, \downarrow\rangle - |\downarrow, \uparrow\rangle] + 0.99049 |\uparrow\downarrow, 0\rangle + 0.00950725 |0, \uparrow\downarrow\rangle, \quad (14)$$

the first KS excited state, predominantly $|\Psi_1\rangle$, corresponds to a single excitation to a CT state:

$$|\Phi_{e1}^{cs-cs}\rangle = 0.980985 \frac{1}{\sqrt{2}} [|\uparrow, \downarrow\rangle - |\downarrow, \uparrow\rangle] - 0.137236 |\uparrow\downarrow, 0\rangle + 0.137236 |0, \uparrow\downarrow\rangle, \quad (15)$$

and the second KS excited state Φ_{e2}^{cs-cs} is dominated by $|\Psi_3\rangle$ and is actually a double excitation:

$$|\Phi_{e2}^{cs-cs}\rangle = -0.137236 \frac{1}{\sqrt{2}} [|\uparrow, \downarrow\rangle - |\downarrow, \uparrow\rangle] + 0.0095072 | \uparrow\downarrow, 0 \rangle + 0.990492 |0, \uparrow\downarrow\rangle. \quad (16)$$

Comparing the KS states with the interacting states Eqs. (11-13) we see they are very similar.

Table I contains the energies, site-occupation differences $\Delta n = \langle \Psi^{cs-cs} | \hat{\Delta n} | \Psi^{cs-cs} \rangle$ of the three interacting and KS states enumerated in Eqs. (11-16), and the transition matrix elements from the gs to the CT excited states, $d_{gs \rightarrow e1(2)} = \langle \Psi_{e1(2)}^{cs-cs} | \hat{\Delta n} | \Psi_{gs}^{cs-cs} \rangle$ for both interacting and Kohn Sham systems. By construction the exact gs HXC functional E_{HXC} reproduces the exact gs energy E_{gs} and gs density Δn_{gs} . All other KS variables shown such as interacting excitation frequencies ω^S and transition matrix elements $d_{gs \rightarrow e1(2)}^S$ have limited physical

TABLE I. Eigenstates, energies, and transition matrix elements for the dimer with $\Delta v^0 = -1.5 U$, $T = 0.05$, $U = 1$. Energies are given in units of U . Note that $e1$ and $e2$ are CT excitations for both the interacting and KS systems.

	$\Delta v = -1.5 U$	
	interacting	Kohn-Sham
Δn_{gs}	1.9620	1.9620
E_{gs}	-0.5098	-0.5098
ϵ_{gs}		-0.5152
Δn_{e1}	0.0364	0.0000
ϵ_{e1}	0.0078	0.0000
$\omega_{gs \rightarrow e1}$	0.5177	0.5152
$d_{gs \rightarrow e1}$	-0.2733	-0.2745
Δn_{e2}	-1.9980	-1.9620
ϵ_{e2}	2.5020	0.5152
$\omega_{gs \rightarrow e2}$	3.0118	1.0304
$\omega_{e1 \rightarrow e2}$	2.4942	0.5152
$d_{gs \rightarrow e2}$	-0.0052	0.0000
$d_{e1 \rightarrow e2}$	-0.0563	-0.2745

meaning. For the case of the cs-cs CT we are studying in this section however, they turn out to be good approximations to the exact quantities, $\omega_{e(2)}^s = \epsilon_{e(2)}^s - \epsilon_{gs}^s \approx \omega$, and $d_{gs \rightarrow e1(2)}^s = \langle \Phi_{gs} | \hat{\Delta n} | \Phi_{e(2)} \rangle \approx d_{gs \rightarrow e1(2)}$. However, in contrast to the interacting system the non-interacting Kohn-Sham system has equidistant excitations $\epsilon_{e2}^s - \epsilon_{e1}^s = \epsilon_{e1}^s - \epsilon_{gs}^s$. That is, the second KS excitation is a pure double-excitation out of the doubly-occupied gs KS orbital; consequently, its dipole transition matrix element is exactly zero. In the interacting system, the second excitation has a very small but non-zero transition matrix element (see Table I). We will choose a field resonant with the first excitation, weak enough that only the ground and first excited interacting states get occupied during the dynamics.

We induce the CT dynamics by turning on a field resonant with the lowest excitation, $\mathcal{E}(t) = 0.09 \sin(\omega t)$, with $\omega = \omega_{gs \rightarrow e1} = 0.5177 U$. All propagations were performed using the Crank-Nicholson scheme and a time-step of $0.01/U$. We evolve the interacting gs in the Hamiltonian of Eq. 1 to obtain the exact dipole shown in the lower part of Figure 4 for a little over half a Rabi period; the CT excited state is reached at around $t = 128/U$. The physics is similar to the real-space CT dynamics in the long-range one-dimensional molecule shown in Figure 4 of Ref. [14] (see also Figure 3 in Ref. [22]) [41] and also in the three-dimensional LiCN molecule in Figures 3 and 4 in Ref. [13]. Fig. 4 shows also the dipole under propagation with the adiabatic exchange (AEXX) approximation, $\Delta v_{HXC}^{AEXX} = \Delta v_{HX} = 2 \frac{\partial E_{HX}[\Delta n]}{\partial \Delta n} = \frac{U}{2} \Delta n(t)$ [27]. Δn_{sc}^{AEXX} does not show any charge-transfer, resembling the real-space AEXX case

of Ref. [14]. Other adiabatic approximations were also shown to fail in a similar way [13, 14]. However in Refs. [13, 14] it was not possible to determine whether the culprit was the adiabatic approximation itself or the chosen gs approximation. For the Hubbard dimer, with its vastly reduced Hilbert space, and the exact HXC potential found by the constrained search (section II) we are able to propagate the KS system with the AE functional; at each time-step inserting the instantaneous density Δn_{sc}^{AE} into the exact gs HXC potential $\Delta v_{HXC}^{gs}[\Delta n_{sc}^{AE}]$ (Fig. 3). The result is Δn_{sc}^{AE} on the bottom of Fig. 4: Δn_{sc}^{AE} closely follows the exact density for a longer time than the AEXX does, but ultimately fails to transfer the charge. As was concluded in Ref. [22], it is essential to have a memory-dependent functional in order to correctly describe a full charge transfer.

Ref. [22] plotted the exact and AE potentials for the case of cs-cs CT studied there, which illuminated some of the aspects of the dynamics, and strengthened the comparison with the real-space molecular case. Although the case studied in Ref. [22] was for a more asymmetric dimer ($\Delta v = -2$), resulting in a higher resonant field frequency and more oscillations over the Rabi period, the essential observations carry over to the present case, and the potentials follow similar features to those shown in Ref. [22]. In particular, (i) the exact correlation potential drops from its gs value to that of $-\Delta v^0$ after half a Rabi cycle, such that the total KS potential $\Delta v_s = \Delta v^0 + \Delta v_{HXC}$ goes to zero, equalizing the levels on each site. This exactly mirrors the real-space case, where a spatial step in the correlation potential in the intermolecular bonding region develops such that at half-Rabi cycle, the two atomic levels are aligned with each other, i.e. the step has a size equal to the difference in the ionization potentials of the $(N - 1)$ -electron ions. (ii) The AE correlation potential evaluated on the *exact* density, $\Delta n^{AE}[\Delta n]$, tracks the ground-state correlation potential shown in Fig. 3, moving from the right inwards to the central region, gently oscillating around it, in synch with the density. As $\Delta n(t) \rightarrow 0$ and the CT state is reached it tracks the approaching discontinuity, which in the limit of $T/U \rightarrow 0$, is equal to the one-site one-fermion derivative discontinuity [22], in complete analogy with the infinite-separation limit of the real-space molecular case [14]. The donor potential is shifted upwards relative to the acceptor by an amount equal to the derivative discontinuity of the donor, and in both the real-space and Hubbard cases, this underestimates the shift provided by the exact correlation potential. (iii) The self-consistent AE correlation potential, $v_c^{AE}[\Delta n_{sc}](t)$, deviates from the true potential quite early on. As a consequence of this, the two sites remain far from being “aligned”, forbidding the possibility that a stable CT state with one electron on each, can be approached in the self-consistent AE propagation.

We now turn to one aspect of the exact correlation potential that was discussed only briefly in Ref. [22]. It was found that the exact correlation potential af-

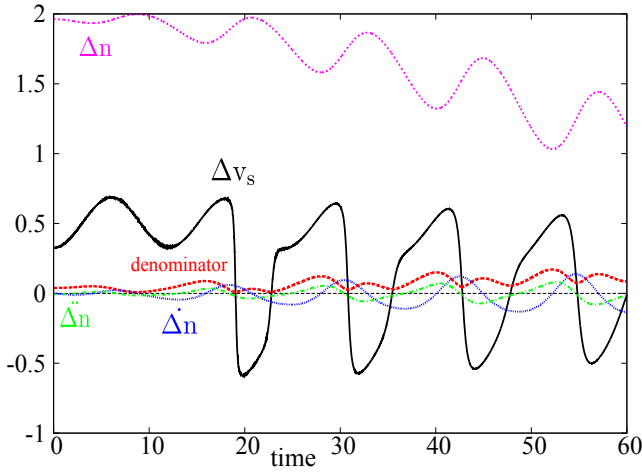


FIG. 5. $\Delta v^0 = -1.5 U$ cs-cs CT: KS potential Δv_s (black solid), denominator of Δv_s (red dashed), link-current Δn (blue dotted), acceleration $\Delta \ddot{n}$ (green dashed-dotted) and dipole Δn (pink dotted).

ter a very short time develops large oscillations which appear to be related to maintaining non-interacting v -representability. Since the system begins with $\Delta n = 1.960$, close to 2, and T is small, the right-hand-side of Eq. 10 starts out quite small. The left-hand-side starts from zero and increases but it does not take a very large link-current for the two sides of Eq. 10 to approach each other, leading to the denominator of Δv_s to approach zero and hence becoming close to violating the non-interacting v -representability condition. Figure 5 shows the early-time behavior of the KS potential: Δv_s first swings sharply to $-\Delta v_s$ (near time of $19/U$) when the denominator gets very close to zero, causing the acceleration $\Delta \ddot{n}$ to change direction (smoothly) and a consequent decrease in the current. This moves the denominator away from zero, escaping the violation of v -representability. The system oscillates due to the field, and again the denominator becomes very small at around time of $22/U$, when again the Δv_s changes direction, avoiding again the crash into non- v -representability. As time evolves the density transfers, Δn moves further from 2, and so larger currents are possible without danger of the v -representability condition being violated. The potential oscillations then become more gentle, as shown in the figure.

IV. OPEN-SHELL TO OPEN-SHELL CT

To study CT between two open-shell fragments we choose the static external potential difference to be $\Delta v^0 = -0.5 U$, which results in a gs with about one electron on each site, $\Delta n = 0.0329$ (see Fig. 6). The value of Δv^0 has been chosen such that $\Delta n_{gs}^{\Delta v=-0.5} \approx \Delta n_{CT}^{\Delta v=-1.5}$ of the cs-cs case in the previous section, and the CT

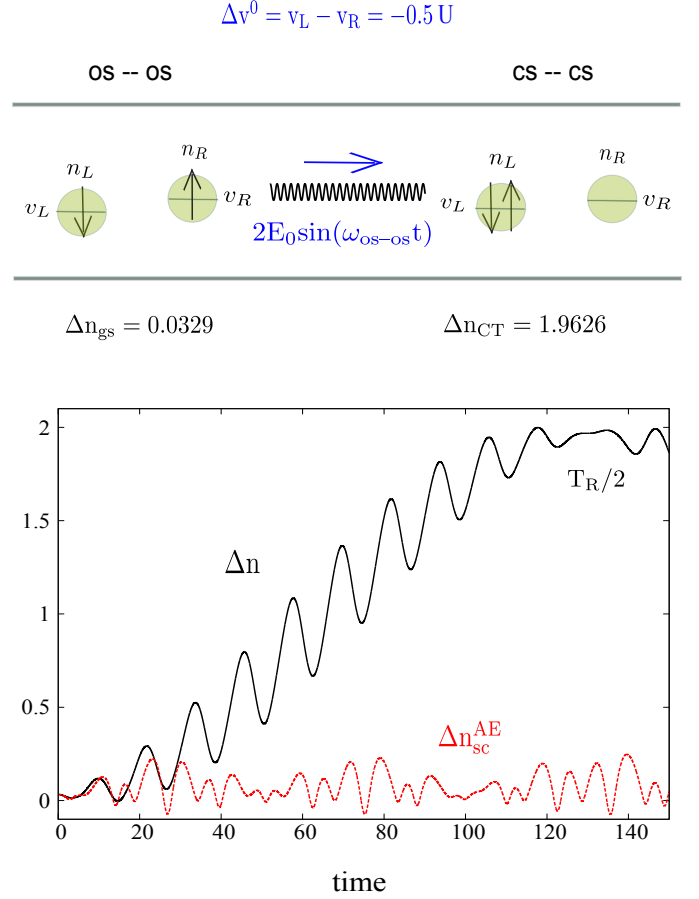


FIG. 6. Model for CT between two open-shell fragments at large separation: a small static potential difference $\Delta v^0 = -0.5 U$, is chosen such that the gs is close to homogenous ($\Delta n_g \approx 0$), and again $T/U = 0.05$. In the bottom panel the results of the propagation are shown: exact dipole $\Delta n(t)$ (black solid), self-consistent AE dipole $\Delta n_{sc}^{AE}(t)$ (red dashed). Time is given in units of $1/U$; the CT state is reached at $T_R/2 \approx 129/U$. (The AEXX dipole is not included, because of difficulties in converging to a stable os-os gs for these parameters).

excitation in the present os-os case has $\Delta n_{CT}^{\Delta v=-0.5} \approx \Delta n_{gs}^{\Delta v=-1.5}$ of the os-os case. (Compare Table I and Table II). The gs of this problem is dominated by $|\Psi_1\rangle$:

$$|\Psi_{gs}^{os-os}\rangle = 0.989568 \frac{1}{\sqrt{2}} [|\uparrow, \downarrow\rangle - |\downarrow, \uparrow\rangle] + 0.136387 |\uparrow\downarrow, 0\rangle + 0.04625 |0, \uparrow\downarrow\rangle, \quad (17)$$

while the CT excited state is mainly $|\Psi_2\rangle$:

$$|\Psi_{e1}^{os-os}\rangle = -0.13608 \frac{1}{\sqrt{2}} [|\uparrow, \downarrow\rangle - |\downarrow, \uparrow\rangle] + 0.99065 |\uparrow\downarrow, 0\rangle - 0.0097168 |0, \uparrow\downarrow\rangle, \quad (18)$$

with almost two electrons on the left site. Again there is a second CT state, with much smaller gs dipole transition matrix element $d_{g \rightarrow CT_2} \ll d_{g \rightarrow CT}$ (see Table II), and close to both electrons on the right ($|\Psi_3\rangle$):

$$|\Psi_{e2}^{os-os}\rangle = -0.0047131 \frac{1}{\sqrt{2}}[|\uparrow, \downarrow\rangle - |\downarrow, \uparrow\rangle] + 0.0033222|\uparrow\downarrow, 0\rangle + 0.99888|0, \uparrow\downarrow\rangle. \quad (19)$$

The ground and excited KS states have a very different form: instead of the predominantly Heitler-London-like nature of the interacting gs, the ground-KS state is a SSD of the form:

$$|\Phi_{gs}^{os-os}\rangle = 0.707011 \frac{1}{\sqrt{2}}[|\uparrow, \downarrow\rangle - |\downarrow, \uparrow\rangle] + 0.50823|\uparrow\downarrow, 0\rangle + 0.49177|0, \uparrow\downarrow\rangle. \quad (20)$$

This is quite analogous to the real-space molecular case where the KS state is a doubly-occupied bonding orbital, a single Slater determinant, while the interacting is of Heitler-London form in the infinite separation limit, requiring minimally two determinants to describe. The KS excitations are also similar to the real-space case: the first KS excitation is not a CT state, but rather a single-excitation to the antibonding state, and second KS excitation is a double-excitation to the antibonding state:

$$|\Phi_{e1}^{os-os}\rangle = -0.016462 \frac{1}{\sqrt{2}}[|\uparrow, \downarrow\rangle - |\downarrow, \uparrow\rangle] + 0.707011|\uparrow\downarrow, 0\rangle - 0.707011|0, \uparrow\downarrow\rangle \quad (21)$$

$$|\Phi_{e2}^{os-os}\rangle = -0.707011 \frac{1}{\sqrt{2}}[|\uparrow, \downarrow\rangle - |\downarrow, \uparrow\rangle] + 0.49177|\uparrow\downarrow, 0\rangle + 0.50823|0, \uparrow\downarrow\rangle. \quad (22)$$

As a consequence the KS excitation energies become very small as $T/U \rightarrow 0$ in contrast with the true energies, just as in the infinite-separation limit of the real-space case, and it can also be understood from the above that the transition matrix elements are large in the KS case while small in the true case (Table II).

We now turn to the dynamics, taking $\mathcal{E}(t) = 0.09 \sin(\omega t)$, resonant with the lowest CT excitation resonance, $\omega = \omega_{gs \rightarrow e1} = 0.5228 U$, and compare the exact and AE dipoles, as in the previous section. Due to the present choice of parameters, the exact dipole looks almost exactly like a mirror image of the cs-cs case in the previous section, i.e. the dipole dynamics in the os-os case resembles that of the cs-cs case starting at the CT state. However the AE dipole does not at all. The AE dipole for the os-os case fails badly even after a very short time, as shown in Fig. 6; for all times one electron

TABLE II. Eigenstates, energies, and transition matrix elements for the dimer with $\Delta v^0 = -0.5 T$, $T = 0.05$, $U = 1$. Energies are given in units of U . Note that $e1$ and $e2$ are CT excitations for the interacting system.

	$\Delta v = -0.5 T$	
	interacting	Kohn-Sham
Δn_{gs}	0.0329	0.0329
E_{gs}	-0.0131	-0.0131
ϵ_{gs}		-0.1000
Δn_{e1}	1.9626	0.000
ϵ_{e1}	0.5097	0.000
$\omega_{gs \rightarrow e1}$	0.5228	0.1000
$d_{gs \rightarrow e1}$	0.2711	1.4140
Δn_{e2}	-1.9955	-0.0329
ϵ_{e2}	1.5033	0.1000
$\omega_{gs \rightarrow e2}$	1.5164	0.2000
$\omega_{e1 \rightarrow e2}$	0.9936	0.1000
$d_{gs \rightarrow e2}$	-0.0915	0.0000
$d_{e1 \rightarrow e2}$	0.0260	1.4140

more or less remains on each site during the AE propagation, while in the exact propagation, (almost) one electron transfers from the left to the right site.

The exact and AE potentials are similar to the os-os case studied in Ref. [22] for a slightly smaller asymmetry ($\Delta v^0 = -0.4$ in Ref. [22]). The essential features are as follows. The exact correlation potential has the same property as in the real-space case: it starts with a value to exactly cancel the asymmetry in the external potential, such that the KS potential sees the two sites aligned. In the real-space case, the HXC gs potential of a long-ranged heteroatomic diatomic molecule has a step in the bonding region that aligns the highest occupied orbital energies on each atom [34–36]. In both real-space and Hubbard dimer cases, this is a ground-state correlation effect. Then, as the charge transfers, the relative shift in the correlation potential between the sites oscillates on the optical scale while dropping to the value predicted by subtracting the external potential from Eq. (9), putting $\dot{\Delta n} = \ddot{\Delta n} = 0$, when the CT excited state is reached. As for $\Delta v_c^{\text{AE}}[\Delta n](t)$, it tracks $\Delta v_c^{\text{gs}}[\Delta n(t)]$ of Fig. 3 moving from near the center out to the right; with gentle oscillations reflecting the oscillations in $\Delta n(t)$. Again we note that its value at the CT excited state is the correlation potential of a gs of density $\Delta n = 1.9626$ as opposed to the exact correlation potential which is that for an excited-state of the same density. On the other hand, the self-consistent AE potential, although it starts correctly (both KS and interacting initial states being ground-states) and captures the relative shift between the sites, quite quickly deviates from the exact. This is because the energy of the

lowest excitation of the KS system is very close to the gs (see Table II); the system becomes increasingly degenerate as $T/U \rightarrow 0$. This is quite in contrast to the true interacting system which has Heitler-London form in the gs and a finite gap $\omega_{gs \rightarrow e1}$. To open the vanishing KS gap $\omega_{gs \rightarrow e1}^s$ strong non-adiabaticity is required in the linear response kernel [37, 38]; the reason is that the double excitation is nearly degenerate with the single excitation and thus critical to incorporate. Given that at short times the dynamics is close to the linear response regime, this might explain why the adiabatic propagation of the os-os system fails so early. Given the analogous structure of the states for a real-space molecule composed of open-shell fragments, we expect that also in real space a self-consistent AE calculation will lead to a very poor dipole.

V. LINEAR RESPONSE FORMULA

The results above show the failure of AE TDDFT to yield accurate CT dynamics in both the case when the CT is between closed-shell sites and when it is between open-shell sites. In the former case we noted that the KS excitation frequencies were close to the exact, while in the latter case they were significantly different. We now ask what the AE TDDFT frequencies are in each case, i.e. when an AE kernel is used in linear response, to check whether there is an indication of the bad CT dynamics of the AE in its predicted excitation energies.

First we derive a general expression for the TDDFT excitation energies of the Hubbard dimer, based on the dipole-dipole response function:

$$\chi_{\Delta n, \Delta n}(\omega) = \frac{d\Delta n}{d(\Delta v/2)} \Big|_{\Delta n_{gs}}, \quad (23)$$

where the factor of $1/2$ comes from the fact that the potential difference couples to the dipole operator $\hat{\Delta n} = \hat{n}_L - \hat{n}_R$ with a factor of $1/2$ in Hamiltonian in Eq. (1). From the relation $\Delta v_s = \Delta v + \Delta v_{\text{HXC}}$, we then find a Dyson-like equation relating $\chi_{\Delta n, \Delta n}(\omega)$ to the KS linear response function and the kernel:

$$\chi_{\Delta n, \Delta n}^{-1}(\omega) = \chi_{s, \Delta n, \Delta n}^{-1}(\omega) - \Delta f_{\text{HXC}}(\omega), \quad (24)$$

where $\Delta f_{\text{HXC}}[\Delta n] = d(\Delta v_{\text{HXC}}[\Delta n]/2)/d(\Delta n)$. In the KS linear response function,

$$\chi_{s, \Delta n, \Delta n}(\omega) = \sum_j \frac{\langle \Phi_{gs} | \hat{\Delta n} | \Phi_{ej} \rangle \langle \Phi_{ej} | \hat{\Delta n} | \Phi_{gs} \rangle}{\omega - \omega_{gs \rightarrow ej} + i\eta} + c.c. \quad (25)$$

there is only one term in the sum, since only one excitation contributes, that due to the KS single-excitation $e1$, as the double-excitation $e2$ yields a zero numerator. At a true excitation, $\chi_{\Delta n, \Delta n}(\omega)$ has a pole in ω , and $\chi_{\Delta n, \Delta n}^{-1}(\omega)$ vanishes. So putting the right-hand-side of

Eq. 24 to zero, we obtain the excitation frequencies of the interacting system from:

$$\omega^2 = \omega_s^2 + 2\omega_s |d_{gs \rightarrow e1}^s|^2 \Delta f_{\text{HXC}}[\Delta n](\omega), \quad (26)$$

where ω_s is the KS eigenvalue difference $\omega_s = \omega_{gs \rightarrow e1}^s$. Eq. (26) has the same form as the “small matrix approximation” of the real-space TDDFT linear response equations [10] except for a factor of 2, again due to the use of Δn as main variable. But an important difference is that Eq. (26) is exact, since there is only one KS single-excitation in the Hubbard dimer. The correction to the bare KS eigenvalue difference (second term in Eq. 26) is most significant for os-os ground states, because, as discussed at the end of section IV, the exact resonant frequency of the interacting os-os system is finite, while the resonant frequency of the KS system is very small (bonding – antibonding transition). As a consequence the exact, frequency-dependent kernel $\Delta f_{\text{HXC}}[\Delta n](\omega)$ must be very large in the os-os case. On the other hand, if we consider the exact gs HXC kernel (shown in inset of Fig. 3), that yields the TDDFT frequency in the AE approximation, it also becomes large around $\Delta n = 0$ (see the inset of Figure 3). That is,

$$\Delta f_{\text{HXC}}^{\text{AE}} = \frac{d(\Delta v_{\text{HXC}}^{\text{gs}}/2)}{d\Delta n} \Big|_{\Delta n_{gs}} = \frac{d^2 E_{\text{HXC}}}{d\Delta n^2} \Big|_{\Delta n_{gs}} \quad (27)$$

has a sharp peaked structure at $\Delta n = 0$. In the limit that $T/U \rightarrow 0$, it becomes proportional to a δ -function. This divergence of the static kernel is consistent with what is found for real os-os molecules at large separation, Refs. [38, 39].

Using Eq. (27) in Eq. (26) gives the AE resonant frequency ω^{AE} . For the $\Delta v^0 = -0.5 U$ os-os CT of section IV we find the AE resonance $\omega_{os-os}^{\text{AE}} = 1.1681 U$ overestimates the physical resonance $\omega_{os-os} = 0.5228 U$ significantly. There is a large non-adiabatic correction to the static kernel in this case. On the other hand, for the cs-cs CT of section III, the bare KS eigenvalue difference is already a good approximation to the true resonance (see table I), and the correction due to $\Delta f_{\text{HXC}}^{\text{AE}}$ brings the AE resonance even closer, $\omega_{cs-cs}^{\text{AE}} = 0.5187 U$, only $0.001 U$ away from the true exact resonance. This is consistent with our finding that for short times, the AE cs-cs dipole followed the exact one closely, while the AE os-os one did not (at short enough times the system responds in a linear way). Similarly in Ref. [13] it was shown that despite good LR spectra (Figure 5), the time-resolved CT within LiCN molecule was not predicted by any of the approximate adiabatic functionals tested. The failure of AE in the cs-cs case at later times is not surprising given the fully non-linear nature of the CT dynamics.

These findings are analogous to the real-space case: here CT excitation energies of a long-range molecule composed of closed-shell fragments can be well-captured by an adiabatic approximation (e.g. Ref. [40]), but the non-linear process of fully time-resolved CT, requires a non-adiabatic approximation. When the

molecule consists of two open-shell fragments, non-adiabaticity is essential even in the linear response regime [38].

VI. CONCLUSIONS AND OUTLOOK

The Hubbard dimer with small T/U parameters is useful for studying real-time CT dynamics in a long-range molecule. Due to its small Hilbert space much can be done numerically exactly or even analytically, so enabling a thorough study of the performance of the adiabatic approximation in TDDFT, which can not be easily studied in real-space. In particular, we examined here the performance of the AE propagation to describe time-resolved CT dynamics. Although previous work on real-space molecules has shown that the usual adiabatic approximations perform poorly [13], whether this is largely due to the choice of gs functional or to the adiabatic approximation itself was not known. Ref. [14] showed that the AE approximation when evaluated on the *exact* density, yields a step structure known to be important in CT dynamics. This AE step has exactly the right size in the case of CT between two open-shell atoms, where the step appears in the initial potential, but the wrong step-size for CT between two closed-shell atoms when the step appears in the final CT excited state. By propagating the Hubbard dimer self-consistently with the AE approximation, a numerically very challenging task in real-space, we were able to show that the AE approximation qualitatively fails to describe time-resolved CT dynamics. In the case of CT between open-shell fragments AE fails very early, and actually does not transfer any charge. In the case of CT between closed-shells the collapse of the adiabatic approximation shows up later in the dynamics: the AE dipole follows the exact one for a significant part of the Rabi cycle, but it drops back to its initial value way before the physical system has reached the CT state. One may think that the failure is due to the AE resonant frequency being detuned from the exact one, but for the cs–cs case the AE resonance is actually very close to the exact resonance! Clearly memory effects are essential to describe time-resolved CT.

In both the cs–cs CT and the os–os CT, the form of the interacting state undergoes a fundamental change:

in the cs–cs case, from approximately a single-Slater determinant initially to a double-Slater determinant of Heitler-London type in the CT state, while the reverse occurs for the os–os case. The KS state however remains a single Slater determinant throughout (a doubly-occupied orbital singlet state). In a sense, this is the underlying reason for the development (or loss) of the step structure in the exact potential in real-space, reflected in the Hubbard model by the realignment of the two sites, signifying strong correlation. An AE approximation does capture this strong correlation effect perfectly when it occurs in the gs, but our work here shows it cannot propagate well. In the cs–cs case, the AE potential was ultimately unable to develop the shift needed for the CT state. In the os–os case it begins with the correct shift but the near-degeneracy in the KS system meant that even as soon as we begin to evolve away from the gs, the AE approximation fails. The main features of the exact time-dependent HXC potential and the exact gs potential are analogous to the real-space case, in particular the relative shifts between donor and acceptor and the relation with the derivative discontinuity. This shift appears as an intermolecular step in the real-space case, but we show here that an ‘adiabatic step’ is not enough to model the dynamics: the results here suggest that its nonlocal dependence on both space and time must be modelled to yield accurate CT dynamics in molecules.

Of course there are many aspects of a real CT within a molecule that cannot be modeled by a two-site lattice, nevertheless we stress here that even for such a simple model relevant physics of the electronic process is missed if an adiabatic approximation is used. The impact of the step structure is likely to be dampened by the effect of many electrons, three-dimensions, coupling to ionic motion, etc, but there is no reason to believe that the shortcomings of the adiabatic approximation to describe time-resolved long-range CT will completely disappear when more complexity is added to the model.

ACKNOWLEDGMENTS

We gratefully acknowledge financial support from the National Science Foundation CHE-1152784 (NTM) and US Department of Energy Office of Basic Energy Sciences, Division of Chemical Sciences, Geosciences and Biosciences under Award DE-SC0008623 (JIF).

-
- [1] W. R. Duncan and O. V. Prezhdo, *Annu. Rev. Phys. Chem.* **58**, 143 (2007).
 - [2] A. E. Jilaubekov et al., *Nature Mat.* **12**, 66 (2012).
 - [3] E. Tapavicza et al., *J. Chem. Phys.* **129**, 124108 (2008).
 - [4] D. Polli et al., *Nature* **467**, 440 (2010).
 - [5] A. Nitzan and M. A. Ratner, *Science* **300**, 1384 (2003).
 - [6] C. A. Rozzi et al., *Nature Comm.* **4**, 1602 (2013)
 - [7] G. Sansone et al., *Nature* **465**, 763 (2010);
 - [8] Y. Suzuki et al., arxiv: 1311.3218
 - [9] E. Runge and E.K.U. Gross, *Phys. Rev. Lett.* **52**, 997 (1984).
 - [10] *Fundamentals of Time-Dependent Density Functional Theory*, (*Lecture Notes in Physics* 837), eds. M.A.L. Marques, N.T. Maitra, F. Nogueira, E.K.U. Gross, and A. Rubio, (Springer-Verlag, Berlin, Heidelberg, 2012).
 - [11] *Time-dependent Density-Functional Theory*, C.A. Ullrich, (Oxford University Press, 2012)

- [12] T. Stein, L. Kronik, R. Baer, J. Am. Chem. Soc. **131**, 2818 (2009); R. Baer, E. Livshitz, U. Salzner, Annu. Rev. Phys. Chem. **61**, 85 (2010).
- [13] S. Raghunathan and M. Nest, J. Chem. Theory and Comput. **7**, 2492 (2011).
- [14] J. I. Fuks, P. Elliott, A. Rubio, and N. T. Maitra, J. Phys. Chem. Lett. **4**, 735 (2013).
- [15] M. Ruggenthaler and D. Bauer, Phys. Rev. Lett. **102**, 233001 (2009).
- [16] J. I. Fuks, N. Helbig, I.V. Tokatly and A. Rubio, Phys. Rev. B **84**, 075107 (2011).
- [17] P. Elliott, J. I. Fuks, A. Rubio, and N. T. Maitra, Phys. Rev. Lett. **109**, 266404 (2012).
- [18] M. Thiele, E. K. U. Gross, and S. Kümmel, Phys. Rev. Lett. **100**, 153004 (2008).
- [19] M. Thiele, S. Kümmel, Phys. Rev. A **79**, 052503 (2009).
- [20] R. Requist, O. Pankratov, Phys. Rev. A **81**, 042519 (2010).
- [21] K. Luo et al. submitted to J. Chem. Phys. (2013), arXiv:1312.1932
- [22] J.I. Fuks, N. T. Maitra, arxiv.org/abs/1312.6880
- [23] F. Aryasetiawan and O. Gunnarsson, Phys. Rev. B **66**, 165119 (2002).
- [24] C. Verdozzi, Phys. Rev. Lett. **101**, 166401 (2008).
- [25] D. J. Carrascal, J. Ferrer, Phys. Rev. B **85**, 045110 (2012).
- [26] Li, Y., Ullrich, C., J. Chem. Phys. **129**, 044105 (2008).
- [27] K. Capelle and V. L. Campo Jr., Phys. Rep. **528**, 91 (2013).
- [28] J. I. Fuks, M. Farzanehpour, I.V. Tokatly, H. Appel, S. Kurth, A. Rubio Phys. Rev. A **88** 062512 (2013)
- [29] M. Farzanehpour, I. V. Tokatly, Phys. Rev B **86**, 125130 (2012).
- [30] R. Baer, J. Chem. Phys. **128**, 044103 (2008).
- [31] P. Hohenberg and W. Kohn, Phys. Rev. **116**, B864 (1964).
- [32] M. Levy, Phys. Rev. A **26**, 1200 (1982).
- [33] E.H. Levy, Int. J. Quantum Chem. **24**, 243 (1983).
- [34] Perdew, J. P. in *Density Functional Methods in Physics*, edited by Dreizler R.M. and da Providencia, J.; Plenum: New York, 1985.
- [35] O. V. Gritsenko, and E. J. Baerends, Phys. Rev. A **54**, 1957 (1996).
- [36] D.G. Tempel, T. J. MartÍnez, and N. T. Maitra, J. Chem. Theory and Comput. **5**, 770 (2009).
- [37] P. Elliott, S. Goldson, C. Canahui, N.T. Maitra, Chem. Phys. **391**, 110 (2011)
- [38] N. T. Maitra and D. G. Tempel, J. Chem. Phys. **126**, 184111 (2006).
- [39] O. V. Gritsenko, S. J. A. van Gisbergen, A. Görling, E. J. Baerends, J. Chem. Phys. **113**, 8478 (2000).
- [40] O. Gritsenko and E. J. Baerends, J. Chem. Phys. **121**, 655 (2004).
- [41] Figure 3 of Ref. [22], which was for the Hubbard dimer with a larger asymmetry, happens to have a closer match with the real-space case. The resonant frequency was larger, so the dipole oscillates faster in the half-Rabi period and also the transition matrix element $d_{gs \rightarrow e1}$ was smaller, making the amplitude of the fast oscillations smaller.